ACS APPLIED NANO MATERIALS

www.acsanm.org Article

Magnesia and Magnesium Aluminate Catalyst Substrates for Carbon Nanotube Carpet Growth

Xu Li, Eric R. Gray, Ahmad E. Islam, Gordon A. Sargent, Benji Maruyama, and Placidus B. Amama*

Cite This: *ACS Appl. Nano Mater.* 2020, 3, 1830−1840 Read Online

ACCESS | Metrics & More | Article Recommendations | Supporting Information

ABSTRACT: Carbon nanotube (CNT) carpet growth behavior is systematically investigated on a pristine and ion beam-bombarded family of basic catalyst substrates: $MgAl_2O_4$ (100), $MgAl_2O_4$ (110), $MgAl_2O_4$ (111), and MgO (100). Interrelationships between physicochemical properties of catalyst substrates (composition, phase, basicity, and surface structure) and CNT carpet growth efficiency (catalyst lifetime and CNT growth rate) for a conventional feedstock (C_2H_4) and an industrial waste (a gaseous product mixture from Fischer−Tropsch synthesis, FTS-GP) as a feedstock are established. Growth on $MgAl_2O_4$ spinel substrates shows ion beam bombardment is effective in transforming "inactive" basic catalyst substrates to "active" substrates that support CNT carpet growth. For "active" catalyst substrates (MgO and ion beam-damaged $MgAl_2O_4$), growth efficiency of a supported catalyst exhibits high sensitivity to the type of feedstock. FTS-GP outperforms C_2H_4 as a feedstock in terms of growth efficiency and the ability of a supported catalyst to promote CNT carpet growth. Superior growth efficiency and CNT quality associated with FTS-GP is attributed to the unique composition of the feedstock that consists of a mixture of hydrocarbons (saturated and unsaturated), nitrogen, and unreacted synthesis gas.

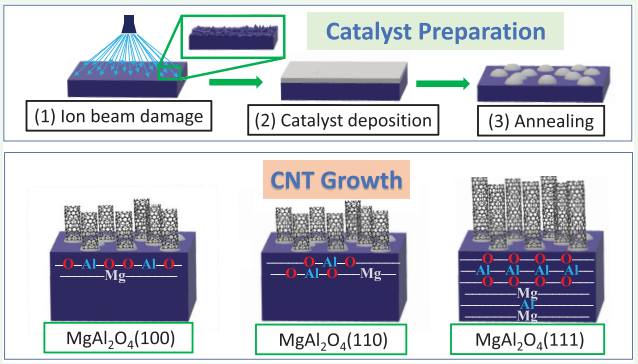

KEYWORDS: *carbon nanotube carpets, carbon nanotube forests, $MgAl_2O_4$, MgO, Fischer−Tropsch synthesis gaseous products*

1. INTRODUCTION

Vertically aligned carbon nanotube (CNT) arrays (or CNT carpets) with controlled properties have received significant attention due to their suitability for a number of applications such as energy storage,[1,2] thermally conductive materials,[3,4] catalysis,[5−7] and sensing devices.[8,9] The preferred method for CNT growth is catalytic chemical vapor deposition (CVD),[10,11] which requires transition metal catalyst (Fe, Co, or Ni) particles supported on an alumina or silica thin film and a carbon feedstock such as a hydrocarbon (C_2H_2, C_2H_4, C_2H_5OH, etc.).[12−14] It is well-known that CNT growth behavior during CVD is sensitive to the type of feedstock and properties of the catalyst substrate.[13,15−18] In the case of substrate properties, important growth steps such as wetting of the catalyst film (during deposition) and dewetting (during annealing and prior to CNT growth) are largely controlled by surface energies of the substrates and the annealing ambient.[19] In fact, physicochemical properties of substrates play a significant role in catalyst particle formation and stability as well as induce different metal−support interactions during CNT growth. Rational substrate design strategies can promote favorable catalyst−support interactions that will maximize CNT carpet growth.

Properties of substrates that profoundly impact CNT growth include chemical composition,[19−21] crystal phase,[22,23] porosity,[13,24] surface energy,[19,25] and surface basicity.[13,15,16,20,26,27] Despite years of research, CNT carpet growth on traditional substrates such as TiO_2,[28,29] ZrO_2,[30] SiO_2,[12,31] and zeolite[32] have largely failed to mimic high-growth efficiency routinely obtained on amorphous alumina films. To broaden catalyst substrates for CNT carpet growth or improve growth efficiency, a variety of strategies have been explored including acid etching[33,34] and plasma etching.[35] Recently, ion beam bombardment has been used for substrate modification prior to catalyst deposition, enabling transformation of "inactive" substrates such as c-cut sapphire and stainless steel to "active" substrates for CNT growth.[36−38] In the case of sapphire, the transformation is attributed to the creation of surface porosity and Lewis basicity after modification. In spite of these promising developments, interrelationships between substrate modification, substrate properties, and type of feedstock are yet to be investigated. To enhance scalability of CNTs and sustainability of the growth process as well as lower production costs, our studies have focused on use of the gaseous product

Received: December 17, 2019
Accepted: February 6, 2020
Published: February 6, 2020

https://dx.doi.org/10.1021/acsanm.9b02509
ACS Appl. Nano Mater. 2020, 3, 1830−1840

mixture from Fischer−Tropsch synthesis (FTS-GP) as a feedstock.[39]

Magnesia and magnesium aluminate ($MgAl_2O_4$) spinel[40,41] are a family of substrates with high basicity and represent a suitable model system for investigating the above interrelationships. MgO has shown anti-sintering and strong catalyst−substrate interactions in Fe-based[42,43] and Co-based[44,45] catalysts. The use of a $MgAl_2O_4$ support in catalysis is quite recent and has been inspired by its unique properties and improved performance of supported catalysts in steam reforming,[46] dehydrogenation reactions,[41] and partial oxidation of methane.[47] In addition, $MgAl_2O_4$ supports a high dispersion of nanosized metal nanoparticles and has the tendency to inhibit formation of carbon impurities and enhance favorable interactions with the metallic phase that inhibits sintering. Further, MgO and $MgAl_2O_3$ consist of large numbers of edges and corners, step edges, and step corners that create basic sites with different strengths depending on the functional group (surface hydroxyl groups and/or low-coordinate O^{2-} sites) that can be utilized for rational catalyst design.[48] The surface structure of complex oxides such as $MgAl_2O_4$ can affect the stability of nanoparticles during film growth.[49]

In this study, the growth behavior of few-walled CNT arrays or small-diameter multiwalled CNTs (MWCNTs) using FTS-GP and a conventional feedstock is systematically investigated on pristine and ion beam-bombarded substrates: $MgAl_2O_4$ (100), $MgAl_2O_4$ (110), $MgAl_2O_4$ (111), and MgO (100). Aligned few-walled CNTs are of interest because they are highly suitable for the production of yarns that exhibit high electrical conductivity and tensile properties.[50,51] Pristine and ion beam-damaged catalyst substrates with different properties (composition, phase, basicity, and surface structure), in combination with either FTS-GP or C_2H_4 as a feedstock, provide a framework to understand complex relationships between substrate properties, types of feedstock, and CNT carpet growth behavior. The use of $MgAl_2O_4$ substrates enables the effects of crystal phase and surface chemistry on the catalytic behavior of an Fe catalyst for substrates of the same composition to be probed, whereas substrate modification of the substrates, conducted using ion beam bombardment,[36,38] enables the effects of surface porosity and basicity to be probed. The results emphasize the critical role of feedstock and provide an incentive for its continued innovation. New catalyst design strategies for efficient CNT carpet growth are also proposed.

2. EXPERIMENTAL SECTION

2.1. Catalyst Preparation. Four pristine and modified substrates were used as catalyst supports for CNT growth via CVD: $MgAl_2O_4$ (100), $MgAl_2O_4$ (110), $MgAl_2O_4$ (111), and MgO (100). The substrates were modified by ion beam bombardment using an ion beam sputter deposition and etching system (IBS/e) from South Bay Technology, Inc. Each substrate was placed directly opposite the Ar ion source (spot size of ∼3 mm) with adjustments made to ensure the beamline was perpendicular to the substrate. Ion beam damage to the substrate was conducted for 10 min at an acceleration voltage of 6 kV and a beam current of 3.5 mA. Total ion dose was calculated to be 1.46×10^{20} cm^{-2}. In calculating the ion dose, its rate was determined by assuming the number of ions injected per unit area per second (N) and the duration of ion exposure (t) were equally received by the substrate. N was calculated using the following equation

$$N = \frac{I}{qA}\ \mathrm{cm}^{-2}\mathrm{s}^{-1} \quad (1)$$

where I is the beam current in amperes, A is the ion beam spot area in square centimeters, and q is the charge of an electron (1.6×10^{-19} Coulomb). Thereafter, Fe catalyst film with a nominal thickness of 2 nm was deposited on the pristine and ion beam-damaged substrates in the IBS/e without exposure to air for the growth of small-diameter MWCNT carpets. Thicknesses of the films deposited were measured by a quartz crystal thickness monitor and corroborated by height profile measurements using an atomic force microscope.

2.2. CNT Growth. The growth of CNT carpets was carried out at atmospheric pressure using an EasyTube 101 CVD system (CVD Equipment Corporation) equipped with a LabView-based process control software, static mixer for optimum gas mixing, and precise temperature-control system. CVD growth was conducted using either ethylene or FTS-GP as a carbon source under conditions optimized for each feedstock. An FTS-GP mixture (supplied by Matheson Inc.) has the following composition: CO (5%), C_2H_6 (8%), C_2H_4 (6%), CH_4 (30%), N_2 (4%), C_3H_8 (5%), H_2 (40%), and C_3H_6 (2%),[52−54] which is identical to a typical composition of a gaseous product mixture from Fischer−Tropsch synthesis and hydrocracking processes in the presence of Fe catalysts.[55] In a typical growth experiment, the catalyst sample was heated to 750 °C at a rate of 50 °C/min in 1000 standard cubic centimeters per minute (sccm) of Ar. For growth with ethylene as a feedstock, catalyst prereduction at the growth temperature (750 °C) was conducted for 10 min with 250 sccm H_2 and 500 sccm Ar. CNT growth was initiated after catalyst prereduction by switching to a gas mixture of 100 sccm C_2H_4, 250 sccm H_2, and 500 sccm Ar. At the completion of growth, samples were rapidly cooled in copious amounts of H_2, followed by slow cooling to room temperature in 700 sccm Ar. For growth using FTS-GP as a feedstock, the catalyst prereduction was conducted by flowing 250 sccm H_2 and 250 sccm Ar. Thereafter, CNT growth was initiated by switching to the growth gas mixture containing 100 sccm FTS-GP and 1000 sccm Ar. At the completion of growth, samples were cooled using the same procedure described above for growth with C_2H_4.

2.3. Characterization. The morphology of the growth products for the different catalyst substrates was characterized with an FEI Quanta scanning electron microscope (SEM) operated at 5 kV. A Nikon Eclipse LV100 optical microscope was also used to measure heights of tall CNT carpets (>35 μm). Transmission electron microscopic (TEM) images were obtained using an FEI Tecnai F20 XT operating at 200 kV. Samples were prepared by dispersing them in ethanol by sonication for 5 min and then dropping them onto a copper microgrid coated with lacy carbon film. Raman spectra of growth products were collected at multiple spots from the samples using a Renishaw inVia Raman microscope equipped with a 514 nm laser (spot size of ∼0.7) as the excitation source. Surface properties of pristine and ion beam-damaged substrates were characterized using X-ray reflectivity (XRR). XRR measurements were conducted on a Rigaku-Smartlab X-ray diffractometer equipped with a Cu Kα (λ = 0.154 nm) radiation source using a slit collimation in air.

3. RESULTS

The CVD growth behavior of an Fe catalyst supported on pristine and ion beam-bombarded substrates [MgO (100), $MgAl_2O_4$ (100), $MgAl_2O_4$ (110), and $MgAl_2O_4$ (111)] with a conventional feedstock (C_2H_4) and FTS-GP was investigated. Figure 1 shows a schematic illustration of the stacking sequence of three, low-index surface orientations of $MgAl_2O_4$[49] as well as catalyst preparation and CNT growth steps. CNT growth efficiency is defined in terms of activity and lifetime of the supported catalyst. Catalytic activity refers to the increase in CNT carpet height with time, while catalyst lifetime is defined as the duration of CNT growth until termination occurs. Morphologies of the resulting products formed on the substrates after exposure to optimum CVD conditions for each feedstock are presented in Figure 2. SEM images in Figure 2a,b show CNTs formed on pristine substrates after 10 min using C_2H_4 and FTS-GP as a feedstock, respectively. For CNTs

https://dx.doi.org/10.1021/acsanm.9b02509
ACS Appl. Nano Mater. 2020, 3, 1830−1840

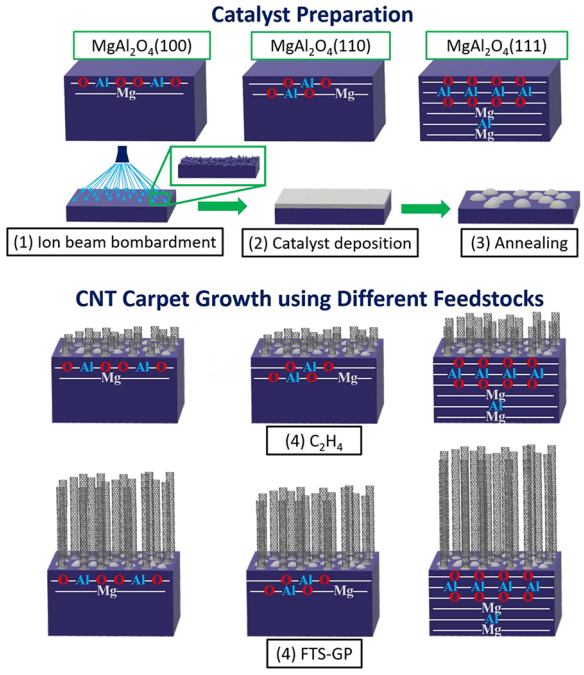

Figure 1. Schematic illustration of the stacking sequence of $MgAl_2O_4$ spinel substrates, the catalyst preparation step, and the CNT growth step using either C_2H_4 or FTS-GP as a feedstock. The catalyst preparation step involves ion beam bombardment of a substrate, deposition of an Fe catalyst film, and annealing of the catalyst prior to CVD growth.

grown with C_2H_4, only MgO (100) substrate supports carpet (or vertically aligned) growth, while growth with FTS-GP yields CNT carpets not only on the MgO (100) substrate but also on one of the spinel substrates [$MgAl_2O_4$ (111)]. For the same growth duration of 10 min using an MgO (100)-supported catalyst, a carpet height of ~400 μm was obtained with FTS-GP, while a lower height of ~300 μm was obtained with C_2H_4, suggesting higher CNT growth efficiency is achieved with FTS-GP. The images reveal catalysts supported on pristine MgO (100) exhibit the highest growth efficiency with full coverage of dense arrays of CNTs across the substrate, a behavior observed irrespective of whether C_2H_4 or FTS-GP is used as a feedstock.

SEM images in Figure 2c,d show CNT carpets formed on ion beam-bombarded substrates after CVD growth with C_2H_4 and FTS-GP, respectively. Coverage of thick CNT carpets was obtained on all ion beam-damaged catalyst substrates, and those exposed to FTS-GP also generally formed taller CNT carpets than those formed with C_2H_4. The positive impact of ion beam bombardment of catalyst substrates on CNT carpet growth is apparent in all the substrates after CVD, especially for $MgAl_2O_4$ (100), $MgAl_2O_4$ (110), and $MgAl_2O_4$ (111) using C_2H_4 as a feedstock and for $MgAl_2O_4$ (100) and $MgAl_2O_4$ (110) using FTS-GP as a feedstock. In these substrates, dense CNT carpet growth became possible only after substrate modification. The dramatic improvement in CNT growth efficiency from catalysts supported on ion beam-damaged substrates further confirms the efficacy of the modification process in the transformation of substrates. As the SEM images in Figure 2 show, ion beam bombardment induces higher CNT nucleation density and growth efficiency for spinel substrates. However, final carpet heights attained after 10 min of growth with either C_2H_4 or FTS-GP from catalysts supported on ion beam-damaged MgO (100) remained roughly the same, suggesting that, unlike $MgAl_2O_4$ substrates, the height of CNT carpet formed on MgO (100) is unaffected by substrate modification. In general, the type of feedstock used during CNT growth significantly affected the activity of the catalyst, with catalysts supported on substrates (pristine or ion beam-damaged) showing substantially higher growth efficiency when FTS-GP is used as a feedstock as opposed to C_2H_4.

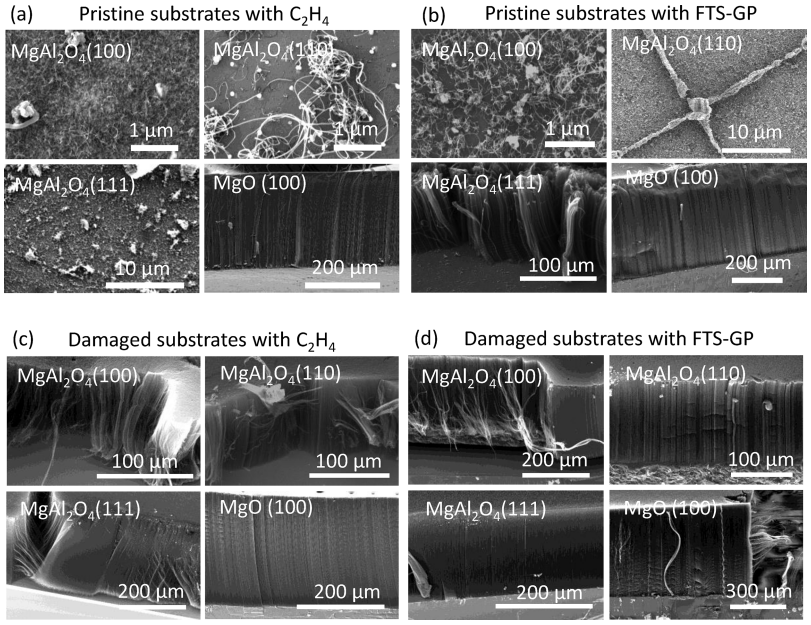

Figure 2. SEM characterization of CNTs grown from Fe catalyst supported on pristine and ion beam-damaged $MgAl_2O_4$ (100), $MgAl_2O_4$ (110), $MgAl_2O_4$ (111), and MgO (100) substrates after 10 min. Images of CNTs formed on pristine substrates using C_2H_4 as a feedstock (a) and FTS-GP as a feedstock (b). Images of CNTs formed on ion beam-bombarded substrates using C_2H_4 as a feedstock (c) and FTS-GP as a feedstock (d).

https://dx.doi.org/10.1021/acsanm.9b02509
ACS Appl. Nano Mater. 2020, 3, 1830−1840

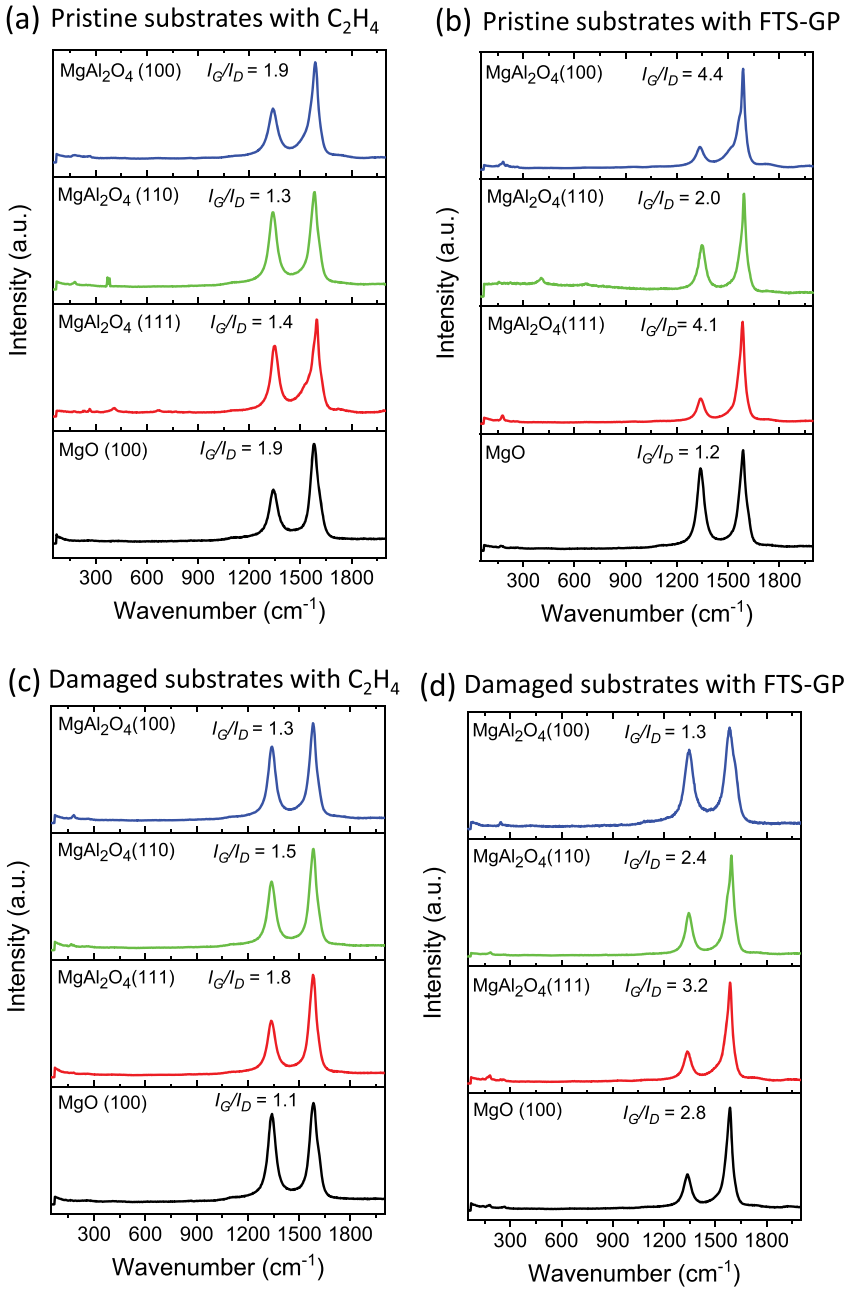

Figure 3. Raman spectroscopic characterization of CNTs grown from an Fe catalyst supported on $MgAl_2O_4$ (100), $MgAl_2O_4$ (110), $MgAl_2O_4$ (111), and MgO (100) catalyst substrates after 10 min. Raman spectra of CNTs formed on a pristine substrate using C_2H_4 as a feedstock (a) and FTS-GP as a feedstock (b). Raman spectra of CNTs formed on ion beam-damaged substrate using C_2H_4 as a feedstock (c) and FTS-GP as a feedstock (d).

Raman spectra of products formed on pristine and ion beam-damaged substrates with either C_2H_4 or FTS-GP as a feedstock are shown in Figure 3. Characteristic modes of CNTs are apparent in the spectra: tangential stretch mode (G-band) at ~1593 cm^{-1} that represents the highly oriented lattice structure of graphitic carbon and disorder-induced mode (D-band) around 1345 cm^{-1} that is indicative of the presence of defects or amorphous carbon. The ratio of G-band to D-band intensities (I_G/I_D), an index to evaluate the quality of the grown CNTs, is shown above each spectrum in Figure 3. In combination with SEM data (Figure 2), the following observation can be gleaned from the Raman spectra: CNTs grown with FTS-GP on all catalyst substrates exhibit higher I_G/I_D, except for pristine MgO (100) and ion beam-damaged $MgAl_2O_4$ (100 and 110).

Further evidence of the difference in structural quality of CNTs grown with FTS-GP and C_2H_4 is provided by TEM images (Figure S1) of CNTs grown on MgO (100). CNTs grown using FTS-GP as a feedstock are of higher quality, evidenced by highly graphitized walls and being largely free of carbon impurities; in contrast, CNTs grown on a similar substrate using C_2H_4 are characterized by significant amounts of carbon impurities on the walls of the tubes. We attribute the higher quality of CNTs obtained with FTS-GP to be due to in situ formation of water that oxidizes excess carbon contaminants. As discussed elsewhere,[56,57] the low concentration of CO in FTS-GP (5 vol % CO) favors the reaction

https://dx.doi.org/10.1021/acsanm.9b02509
ACS Appl. Nano Mater. 2020, 3, 1830−1840

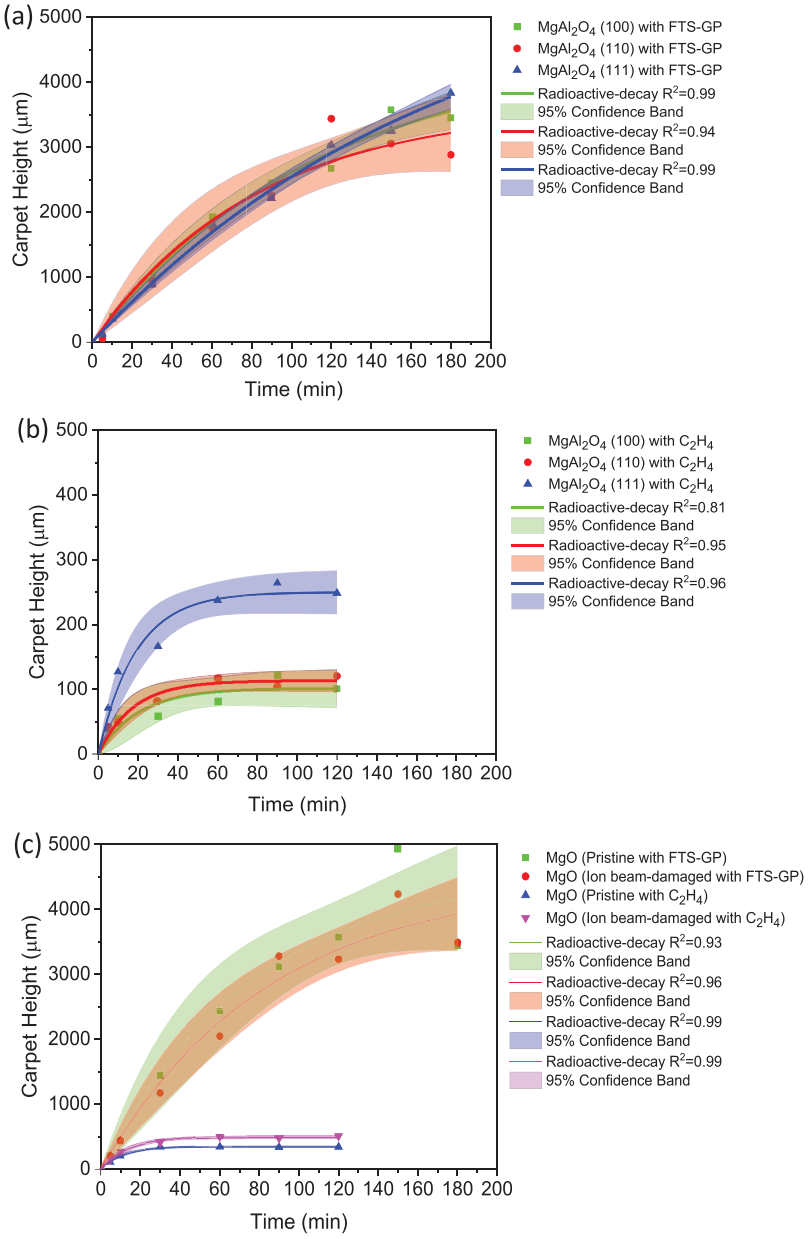

Figure 4. Plots of CNT carpet heights as functions of growth time for ion beam-damaged $MgAl_2O_4$ (100), $MgAl_2O_4$ (110), and $MgAl_2O_4$ (111) catalyst substrates using FTS-GP (a), CNT carpet heights as functions of growth time for ion beam-damaged $MgAl_2O_4$ (100), $MgAl_2O_4$ (110), and $MgAl_2O_4$ (111) catalyst substrates using C_2H_4 (b), and CNT carpet heights as functions of growth time for pristine and ion beam-damaged MgO (100) catalyst substrates (c). Respective shades around the plot show a 95% confidence interval on the fitted data.

between CO and H_2 ($\Delta H = -90$ kJmol^{-1}) to produce water. Improved CNT growth efficiency observed in the spinel substrates after ion beam damage may be due to changes in surface structure and chemistry caused by the modification process; this is consistent with studies that show changes in physicochemical properties affect catalyst−substrate interactions.[27,36] TEM images in Figure S1 reveal tube diameters in the range of 4−10 nm, which is roughly consistent with the catalyst thickness (2 nm-thick Fe film) used in this study. Weak signals of the radial breathing modes (RBMs) observed in most Raman spectra support the possible existence of large-diameter single-walled CNTs (SWCNTs) in combination with small-diameter MWCNTs in the carpets.

Having established substrates that support CNT carpet growth, our next focus is to investigate the growth efficiency of the Fe catalyst supported on "active" substrates (those that support carpet growth). Figure 4 shows plots of CNT carpet height versus growth time (referred to as "growth profiles") for catalysts supported on different supporting layers using C_2H_4 or FTS-GP as a feedstock. The shaded region in each plot shows the 95% confidence interval on the fitted data. In general, the profiles exhibit characteristic features of growth kinetics of CNT carpets with an initial acceleration and an inflection point, followed by gradual deactivation and eventual termination.[58,59] CNT carpet growth using FTS-GP exhibits a higher growth rate and substantially longer catalyst lifetime than carpets obtained with C_2H_4. In Figure 4a, growth with FTS-GP for the three crystalline phases of $MgAl_2O_4$ (100, 110, and 111) exhibited somewhat similar growth profiles in terms of high catalytic activity and resistance to deactivation as the

https://dx.doi.org/10.1021/acsanm.9b02509
ACS Appl. Nano Mater. 2020, 3, 1830−1840

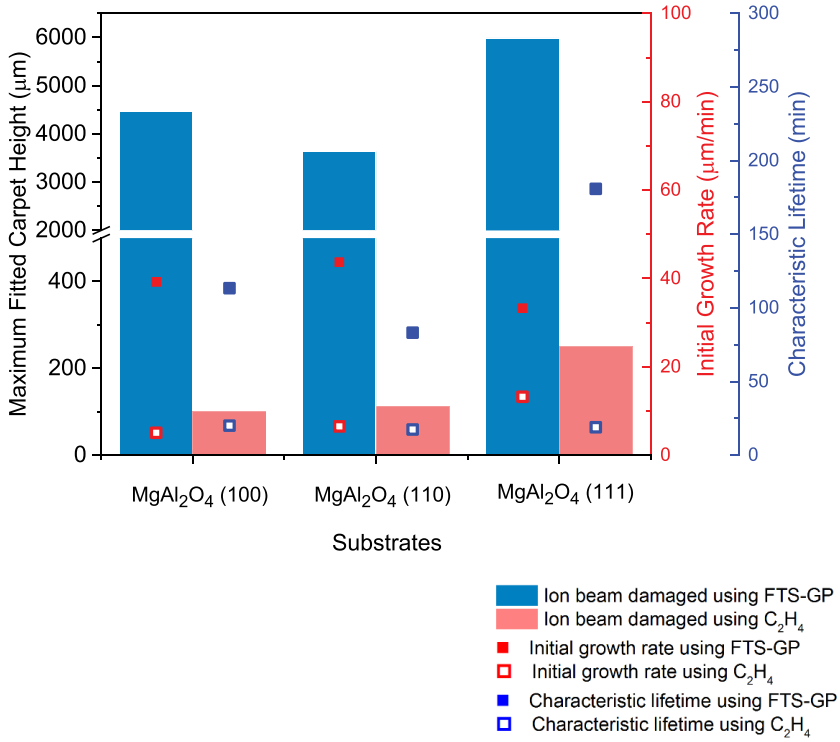

Figure 5. Histogram of maximum fitted carpet heights and scatter plots of the characteristic lifetime (blue squares) and initial growth rate (red squares) as functions of the crystallographic phase of $MgAl_2O_4$ catalyst substrates.

catalysts appear active even after 180 min. On the other hand, growth with C_2H_4 (Figure 4b) exhibited an order of magnitude decrease in catalytic activity with gradual deactivation after ~20 min followed by deactivation after ~100 min; maximum CNT carpet heights attained after 120 min are all in the submillimeter range. Also, unlike FTS-GP, a unique feature of growth using C_2H_4 is the high sensitivity of growth behavior to the crystallographic phase of $MgAl_2O_4$ spinel with growth efficiency decreasing in the following order: $MgAl_2O_4$ (111) > $MgAl_2O_4$ (110) > $MgAl_2O_4$ (100). Figure 4c exhibits growth profiles for catalysts supported on pristine and ion beam-damaged MgO (100) substrates with either FTS-GP or C_2H_4 as a feedstock. Although ion beam bombardment is more effective in transforming an "inactive" substrate to an "active" substrate, growth profiles for MgO (100) substrates clearly confirm the type of feedstock used for growth has a higher impact on growth efficiency of CNT carpets than substrate modification. The superior growth efficiency associated with the use of FTS-GP as a feedstock in carpet growth is also apparent in the growth data.

To compare CNT carpet growth efficiencies of catalysts supported on pristine and ion beam-bombarded substrates, growth data presented in Figure 3 are further analyzed to extract relevant kinetic information. As demonstrated by Futaba et al.,[59] the time evolution of CNT carpet growth can be modeled using the radioactive-decay equation represented by the following differential equation:

$$\frac{\partial H}{\partial t} \propto e^{-t/\tau 0} \tag{2}$$

The integration of eq 2 yields the growth equation:

$$H(t) = \beta\tau_0(1 - e^{-t/\tau_0}) \tag{3}$$

where H is carpet height, t is growth time, β is initial growth rate, and τ_0 is the characteristic lifetime of the catalyst. The product of β and τ_0 is the maximum fitted CNT height (H_{max}).

By fitting our growth data to the radioactive-decay model, we are able to determine β and τ_0, which are fitting parameters that characterize the growth behavior of the catalyst supported on each supporting layer. These fitting parameters have been used to estimate the growth efficiency of CNT carpets. Model equations obtained from the fitting are presented in the Supporting Information, and extracted values for β and τ_0 are summarized in Table S1. Catalysts supported on the ion beam-damaged $MgAl_2O_4$ spinel substrates show initial growth rates and comparable lifetimes, except lifetimes observed for growth with FTS-GP. For growth with FTS-GP, $MgAl_2O_4$(111)/Fe exhibits a lifetime higher than that of $MgAl_2O_4$ (110)/Fe by a factor of 2. A comparison of the two carbon sources used in this study (Figure 4a,b) reveals a stark difference in growth efficiencies. First, FTS-GP outperforms C_2H_4 as a feedstock in terms of initial growth rate and catalyst lifetime for the different ion beam-damaged $MgAl_2O_4$ substrates. It is therefore unsurprising that the growth of CNT carpets with FTS-GP is able to achieve millimeter-tall heights while growth using C_2H_4 yields only submillimeter-tall CNT carpets. Second, among the spinel substrates with different phases, $MgAl_2O_4$ (111) exhibits the highest CNT carpet height, indicating its suitability for efficient CNT carpet growth. The observed CNT growth enhancement with FTS-GP as a feedstock is consistent with growth on alumina-supported catalysts.[56,57]

A summary of the dependence of H_{max}, τ_0, and β on the crystalline phase of $MgAl_2O_4$ spinel is presented in Figure 5. CNT carpets grown on $MgAl_2O_4$ (111) show H_{max} of 5987 μm, which is the highest among all $MgAl_2O_4$ substrates. This trend is also consistent with τ_0, confirming that longer lifetimes are achieved with FTS-GP as a feedstock. $MgAl_2O_4$ (111)

https://dx.doi.org/10.1021/acsanm.9b02509
ACS Appl. Nano Mater. 2020, 3, 1830−1840

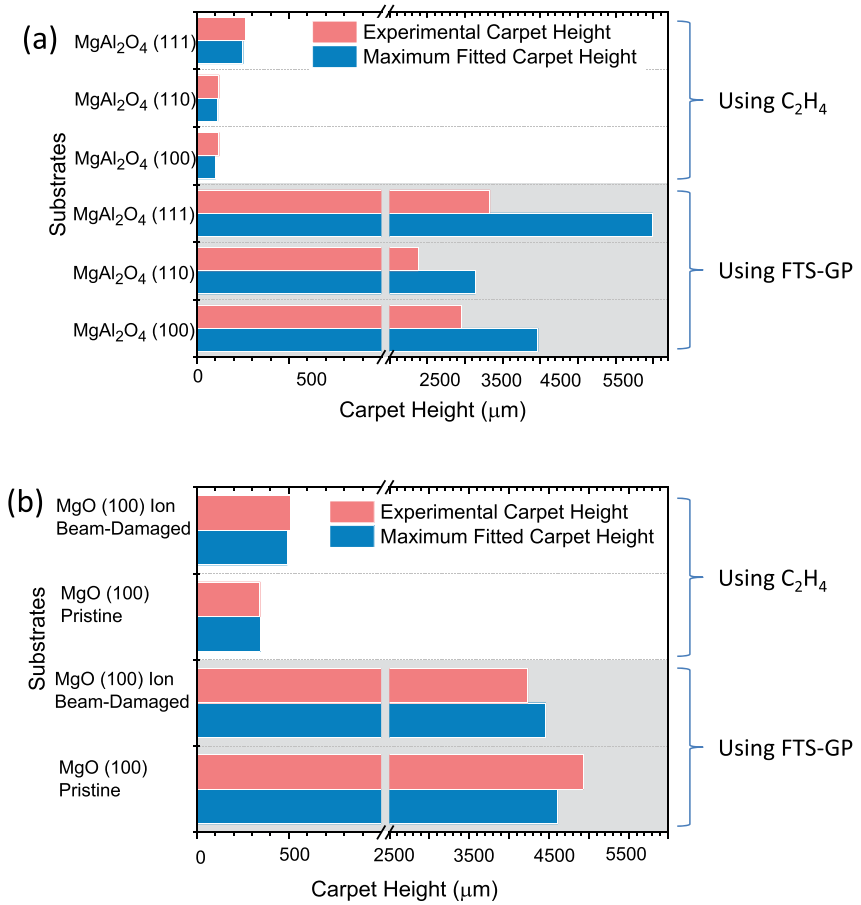

Figure 6. Comparison between theoretical and experimental CNT carpet heights for different catalyst substrates: (a) $MgAl_2O_4$ spinel substrates; (b) MgO (100) substrates.

shows the highest H_{max} in growth experiments utilizing either FTS-GP or C_2H_4 as a feedstock. However, unlike growth with FTS-GP, the growth efficiency of $MgAl_2O_4$ (111)/Fe when C_2H_4 is used as a feedstock is indistinguishable among the spinel substrates in terms of τ_0. This result indicates the type of precursor plays a critical role in extending catalyst lifetime. In fact, a comparison of extracted values for β and τ_0 in Table S1 shows the characteristic lifetime of a catalyst supported on MgO (100) increases by a factor of almost six, while H_{max} increases by a factor of 9 when switching the feedstock from C_2H_4 to FTS-GP.

Figure 6 shows a comparison of maximum fitted and experimental CNT growth results. For CNT carpet growth using FTS-GP, carpet heights from experiments are shorter than maximum fitted carpet heights, indicating catalysts have yet to reach their maximum lifetimes (Figure 6a). Conversely, experimental carpet heights for growth using C_2H_4 are similar to maximum fitted heights, which indicates the catalysts have reached their maximum lifetimes. In Figure 6b, pristine and ion beam-damaged MgO (100) catalyst substrates appear to have reached their maximum catalyst lifetimes because their experimental CNT lengths are very close to H_{max}. From the discrepancy in experimental and maximum fitted CNT carpet heights, we conclude that the combined use of catalysts supported on ion beam-damaged $MgAl_2O_4$ substrates and FTS-GP as a feedstock leads to the longest lifetimes.

XRR measurements were carried out to investigate surface properties of catalyst substrates. XRR interference patterns acquired from pristine and ion beam-damaged $MgAl_2O_4$ spinel and MgO substrates are shown in Figure S2. Fitting the interference fringes with theoretically generated XRR patterns reveals the formation of an upper amorphous layer (Layer 1) and a lower nanocrystalline layer (Layer 2) on top of the crystalline substrate after ion beam bombardment. The detailed steps for extraction of layer thickness and surface roughness are discussed elsewhere.[36] The estimations of roughness and thickness values were not possible for the analyses of some samples due to the large uncertainty. Histograms in Figure 7 show the results of the thickness of the layers and surface roughness extracted from fitting the XRR interference fringes in Figure S2. After ion beam bombardment, the thickness of Layer 1 increased significantly, while that of Layer 2 remained roughly unchanged. From Figure 6, we conclude the overall surface roughness for all substrates, and especially for Layer 2, increases after ion beam bombardment. Surface roughness may also play a role in anchoring catalyst particles, obstructing mobility of catalyst particles on the surface,[60] and extending lifetime. Interestingly, our growth results with FTS-GP support this hypothesis as the catalyst lifetime increases with surface roughness. Surface roughness and τ_0 decrease in the following order: $MgAl_2O_4$ (111) > $MgAl_2O_4$ (100) > $MgAl_2O_4$ (110).

4. DISCUSSION

Our results show the combined use of ion beam-damaged catalyst substrates and FTS-GP as a feedstock results in a

https://dx.doi.org/10.1021/acsanm.9b02509
ACS Appl. Nano Mater. 2020, 3, 1830−1840

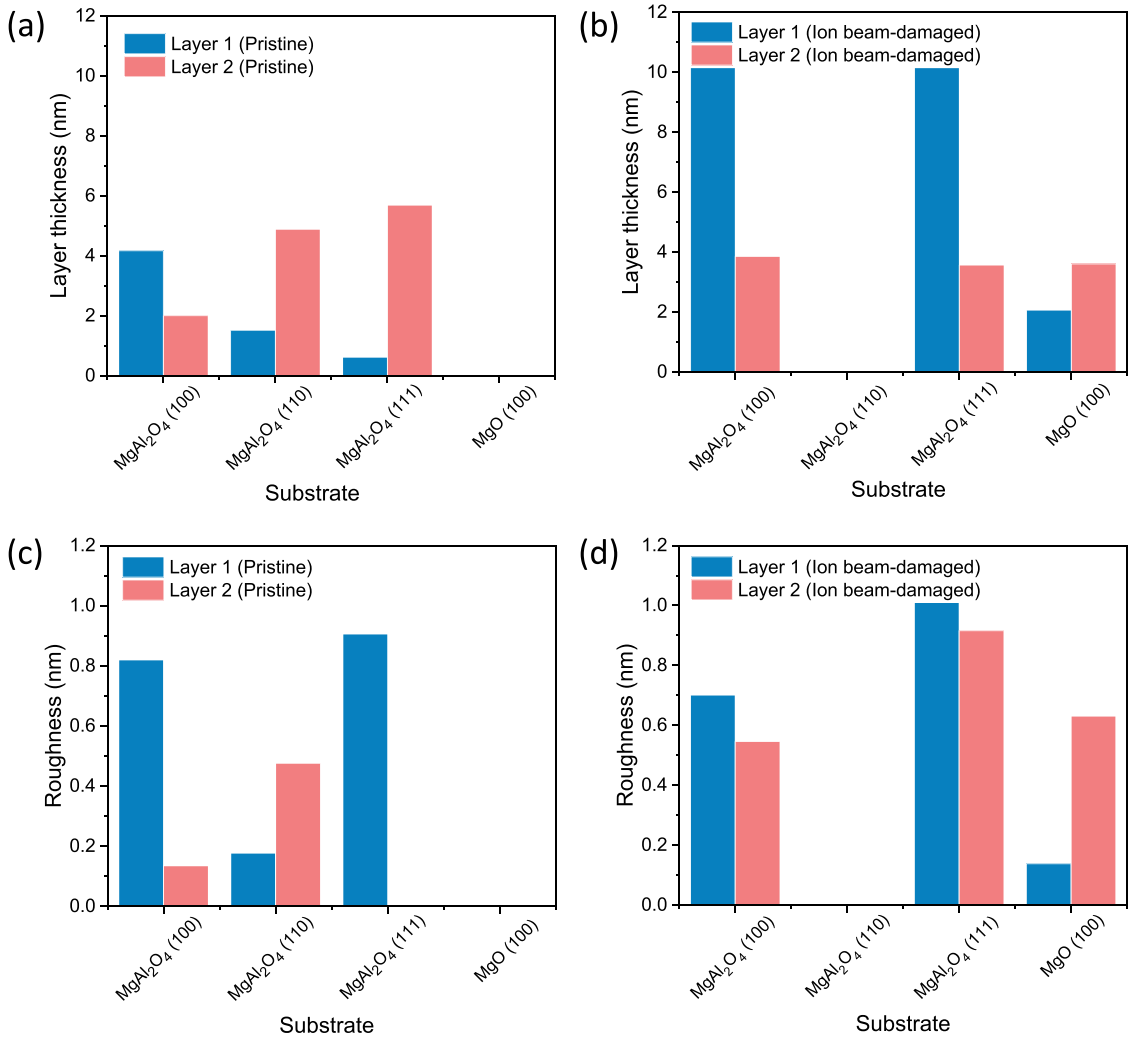

Figure 7. Thickness of different layers present at the surface of pristine (a) and ion beam-bombarded catalyst substrates (b); roughness of different layers present at the surface of pristine (c) and ion beam-bombarded catalyst substrates (d). Data are obtained by fitting XRR patterns in Figure S2.

dramatic improvement in growth efficiency of CNT carpets. The effects of surface-terminating species of spinel substrates, the catalyst preparation step, and the type of feedstock on CNT carpet growth are illustrated in Figure 1. Substrate modification plays a major role in the transformation of "inactive" substrates, while growth efficiency of CNT carpets (on "active" substrates) is largely influenced by the type of feedstock. MgO (100) substrates are "active" for carpet growth, while pristine $MgAl_2O_4$ spinel substrates are "inactive" except for $MgAl_2O_4$ (111) with FTS-GP as a feedstock. The use of ion beam bombardment to modify different "inactive" substrates improved activity of a supported Fe catalyst, which is consistent with previous studies.[37,38] The role of ion beam bombardment is to create porosity and an amorphous-like upper layer as well as increase surface roughness.[36−38] The total effective depth of the amorphous layer is around 10 nm, which allows for mild subsurface diffusion of the catalyst, an important factor for enhanced CNT carpet growth as demonstrated in our previous study.[13] FTS-GP not only shows superior growth efficiency to conventional feedstocks[57] but also shows the ability to induce CNT carpet growth on a basic substrate that is "inactive" as observed in $MgAl_2O_4$ (111). Note that growth efficiency of MgO (100), using FTS-GP as a feedstock, outperforms efficiencies in prior studies where conventional feedstocks were used.[61,62] High surface basicity of MgO and favorable Fe−MgO interactions contribute to the high CNT growth observed on MgO.[27,63,64]

A broad consensus exists in the literature that catalyst substrates with high surface basicity favor CNT growth.[20,27,36,38] The basicities of MgO, Al_2O_3, and $MgAl_2O_4$ have been evaluated by Di Cosimo et al.[65] using CO_2-TPD, and it was found to decrease in the following order: MgO > $MgAl_2O_4$ > Al_2O_3. The high basicity of MgO may be partly responsible for its ability to support good carpet growth in its pristine state while pristine crystalline alumina (c-cut sapphire),[38] with a lower basicity, does not. As shown here and in our prior work,[27,38] growth efficiency of the catalyst on the substrates with comparatively lower basicity ($MgAl_2O_4$ and crystalline sapphire) improves dramatically after ion beam bombardment as it increases hydroxyl enrichment on the surface. Our recent study[37] using a nonoxide catalyst support (316 stainless steel) revealed ion beam bombardment alone is insufficient to induce growth on the substrate; a thin Al_xO_y barrier layer was still required for growth, which supports the hypothesis[14,27,36,38] that a basic surface is favorable for CNT growth.

The superior growth efficiency and CNT quality associated with FTS-GP CVD are attributed to the unique composition of

https://dx.doi.org/10.1021/acsanm.9b02509
ACS Appl. Nano Mater. 2020, 3, 1830−1840

FTS-GP (see Experimental Section) that plays two important roles: (1) FTS-GP enables a high carbon flux from the carbon-rich components to the catalyst "seeds"; (2) a reaction between H_2 and CO is favored, generating water in situ that extends the catalyst lifetime via oxidative removal of amorphous carbon deposited on the catalyst.[66]

Although carpet growth efficiency of the catalysts supported on the $MgAl_2O_4$ spinel substrates shows a high sensitivity to the type of precursor, we also observed a mild sensitivity to the crystallographic phase. Xiong et al.[61] reported a similar finding for MgO whereby a strong dependence of carpet height on the orientation of MgO was demonstrated. To rationalize observed differences in growth behavior, we consider the atomic stacking sequence of different surface orientations of $MgAl_2O_4$ as shown in Figure 1. Unlike the mixed aluminum/oxygen atomic arrangement on the surface of $MgAl_2O_4$ (100) and $MgAl_2O_4$ (110) or magnesium/oxygen (−Mg−O−Mg−O−) in the case of MgO,[67] the top surface of $MgAl_2O_4$ (111) is fully covered with oxygen atoms,[49,68,69] which is evidence of a higher surface basicity than the former substrates and may partly explain its ability to support carpet growth in its pristine state when FTS-GP is used as a feedstock. The different catalytic efficiencies, such as discrepancy in experimental and maximum fitted carpet height, may be due to different interaction energies of Fe with different planes that result in different nucleation behaviors.[61] In addition, surface energies of $MgAl_2O_4$ spinel substrates decrease in the following order: $MgAl_2O_4$ (111) > $MgAl_2O_4$ (110) > $MgAl_2O_4$ (100).[49,68] High surface energy can prevent planar Ostwald ripening and subsurface diffusion.[36] Therefore, the above features of the $MgAl_2O_4$ (111) substrate make it the preferred substrate for CNT carpet growth. Our results show catalyst−substrate interactions and CNT growth behavior are also affected by the different atomic surface arrangements that exist in pristine samples or are formed after ion beam damage.

5. CONCLUSIONS

In conclusion, we have investigated the growth behavior of the Fe catalyst supported on pristine and ion beam-damaged $MgAl_2O_4$ (100), $MgAl_2O_4$ (110), $MgAl_2O_4$ (111), and MgO (100) using either a conventional feedstock (C_2H_4) or FTS-GP as a feedstock. The main finding of this study is the critical role played by catalyst substrate properties and the types of feedstock in CNT carpet growth. Although ion beam bombardment is more effective in transforming an "inactive" basic substrate to an "active" substrate, the type of feedstock used in the growth has a higher impact on CNT carpet growth efficiency (catalyst lifetime and CNT growth rate). FTS-GP outperforms C_2H_4 as a feedstock in terms of growth efficiency, CNT quality, and its ability to support carpet growth. The CNT carpet growth with $MgAl_2O_4$ substrates using FTS-GP shows a discrepancy in experimental and maximum fitted heights, indicating the catalysts have yet to reach a maximum lifetime. Different phases of $MgAl_2O_4$ substrates show slightly different CNT growth behavior due to their different surface chemistries and surface energies. Among the different phases of $MgAl_2O_4$, ion beam-damaged $MgAl_2O_4$ (111) is the best supporting layer, most likely due to its atomic stacking sequence, which makes it highly basic. In addition, the increase in catalyst lifetime with surface roughness suggests the high surface roughness of $MgAl_2O_4$ (111) may be playing a role in anchoring catalyst particles and impeding sintering. The CNT nucleation density of the basic "inactive" substrates can be enhanced by ion beam bombardment, whereas the growth efficiency of CNT carpets can be maximized by the use of FTS-GP as a feedstock.

■ ASSOCIATED CONTENT

Supporting Information

The Supporting Information is available free of charge at https://pubs.acs.org/doi/10.1021/acsanm.9b02509.

Fitting parameters for CNT carpet growth; model equations from fitting; TEM images; XRR profiles (PDF)

■ AUTHOR INFORMATION

Corresponding Author

Placidus B. Amama − *Tim Taylor Department of Chemical Engineering, Kansas State University, Manhattan, Kansas 66506, United States;* orcid.org/0000-0001-9753-6044; Phone: 785-532-4318; Email: pamama@ksu.edu

Authors

Xu Li − *Tim Taylor Department of Chemical Engineering, Kansas State University, Manhattan, Kansas 66506, United States*

Eric R. Gray − *Tim Taylor Department of Chemical Engineering, Kansas State University, Manhattan, Kansas 66506, United States*

Ahmad E. Islam − *Materials and Manufacturing Directorate, Air Force Research Laboratory, Wright-Patterson Air Force Base, Ohio 45433, United States*

Gordon A. Sargent − *Materials and Manufacturing Directorate, Air Force Research Laboratory, Wright-Patterson Air Force Base, Ohio 45433, United States*

Benji Maruyama − *Materials and Manufacturing Directorate, Air Force Research Laboratory, Wright-Patterson Air Force Base, Ohio 45433, United States*

Complete contact information is available at: https://pubs.acs.org/10.1021/acsanm.9b02509

Notes

The authors declare no competing financial interest.

■ ACKNOWLEDGMENTS

We acknowledge funding from the National Science Foundation (Grant Number: 1728567) and access to material characterization facilities at AFRL through an Educational Partnership Agreement. The authors are grateful to Brian Everhart for assisting with the graphic design.

■ REFERENCES

(1) Wang, W.; Kumta, P. N. Nanostructured hybrid silicon/carbon nanotube heterostructures: reversible high-capacity lithium-ion anodes. *ACS Nano* **2010**, *4* (4), 2233−2241.

(2) Pint, C. L.; Nicholas, N. W.; Xu, S.; Sun, Z.; Tour, J. M.; Schmidt, H. K.; Gordon, R. G.; Hauge, R. H. Three dimensional solid-state supercapacitors from aligned single-walled carbon nanotube array templates. *Carbon* **2011**, *49* (14), 4890−4897.

(3) Chen, H.; Chen, M.; Di, J.; Xu, G.; Li, H.; Li, Q. Architecting three-dimensional networks in carbon nanotube buckypapers for thermal interface materials. *J. Phys. Chem. C* **2012**, *116* (6), 3903−3909.

(4) Cola, B. A.; Xu, J.; Cheng, C.; Xu, X.; Fisher, T. S.; Hu, H. Photoacoustic characterization of carbon nanotube array thermal interfaces. *J. Appl. Phys.* **2007**, *101* (5), 054313.

(5) Almkhelfe, H.; Li, X.; Thapa, P.; Hohn, K. L.; Amama, P. B. Carbon nanotube-supported catalysts prepared by a modified photo-Fenton process for Fischer−Tropsch synthesis. *J. Catal.* **2018**, *361*, 278−289.
(6) Li, W.; Liang, C.; Zhou, W.; Qiu, J.; Zhou, Z.; Sun, G.; Xin, Q. Preparation and characterization of multiwalled carbon nanotube-supported platinum for cathode catalysts of direct methanol fuel cells. *J. Phys. Chem. B* **2003**, *107* (26), 6292−6299.
(7) Gong, K.; Du, F.; Xia, Z.; Durstock, M.; Dai, L. Nitrogen-doped carbon nanotube arrays with high electrocatalytic activity for oxygen reduction. *Science* **2009**, *323* (5915), 760−764.
(8) Saetia, K.; Schnorr, J. M.; Mannarino, M. M.; Kim, S. Y.; Rutledge, G. C.; Swager, T. M.; Hammond, P. T. Spray-Layer-by-Layer Carbon Nanotube/Electrospun Fiber Electrodes for Flexible Chemiresistive Sensor Applications. *Adv. Funct. Mater.* **2014**, *24* (4), 492−502.
(9) Llobet, E. Gas sensors using carbon nanomaterials: A review. *Sens. Actuators, B* **2013**, *179*, 32−45.
(10) Baker, R. Catalytic growth of carbon filaments. *Carbon* **1989**, *27* (3), 315−323.
(11) Shah, K. A.; Tali, B. A. Synthesis of carbon nanotubes by catalytic chemical vapour deposition: A review on carbon sources, catalysts and substrates. *Mater. Sci. Semicond. Process.* **2016**, *41*, 67−82.
(12) Mattevi, C.; Wirth, C. T.; Hofmann, S.; Blume, R.; Cantoro, M.; Ducati, C.; Cepek, C.; Knop-Gericke, A.; Milne, S.; Castellarin-Cudia, C.; et al. In-situ X-ray photoelectron spectroscopy study of catalyst- support interactions and growth of carbon nanotube forests. *J. Phys. Chem. C* **2008**, *112* (32), 12207−12213.
(13) Amama, P. B.; Pint, C. L.; Kim, S. M.; McJilton, L.; Eyink, K. G.; Stach, E. A.; Hauge, R. H.; Maruyama, B. Influence of Alumina Type on the Evolution and Activity of Alumina-Supported Fe Catalysts in Single-Walled Carbon Nanotube Carpet Growth. *ACS Nano* **2010**, *4* (2), 895−904.
(14) Magrez, A.; Smajda, R.; Seo, J. W.; Horvath, E.; Ribič, P. R.; Andresen, J. C.; Acquaviva, D.; Olariu, A.; Laurenczy, G.; Forró, L. s. Striking influence of the catalyst support and its acid-base properties: new Insight into the growth mechanism of carbon nanotubes. *ACS Nano* **2011**, *5* (5), 3428−3437.
(15) Wang, Y.; Luo, Z.; Li, B.; Ho, P. S.; Yao, Z.; Shi, L.; Bryan, E. N.; Nemanich, R. J. Comparison study of catalyst nanoparticle formation and carbon nanotube growth: support effect. *J. Appl. Phys.* **2007**, *101* (12), 124310.
(16) Ward, J.; Wei, B.; Ajayan, P. Substrate effects on the growth of carbon nanotubes by thermal decomposition of methane. *Chem. Phys. Lett.* **2003**, *376* (5−6), 717−725.
(17) Lee, T. Y.; Han, J.-H.; Choi, S. H.; Yoo, J.-B.; Park, C.-Y.; Jung, T.; Yu, S.; Lee, J.; Yi, W.; Kim, J. M. Comparison of source gases and catalyst metals for growth of carbon nanotube. *Surf. Coat. Technol.* **2003**, *169−170*, 348−352.
(18) Sugime, H.; Noda, S. Cold-gas chemical vapor deposition to identify the key precursor for rapidly growing vertically-aligned single-wall and few-wall carbon nanotubes from pyrolyzed ethanol. *Carbon* **2012**, *50* (8), 2953−2960.
(19) Dupuis, A.-C. The catalyst in the CCVD of carbon nanotubes—a review. *Prog. Mater. Sci.* **2005**, *50* (8), 929−961.
(20) Vander Wal, R. L.; Ticich, T. M.; Curtis, V. E. Substrate-support interactions in metal-catalyzed carbon nanofiber growth. *Carbon* **2001**, *39* (15), 2277−2289.
(21) Amama, P. B.; Pint, C. L.; Mirri, F.; Pasquali, M.; Hauge, R. H.; Maruyama, B. Catalyst-support interactions and their influence in water-assisted carbon nanotube carpet growth. *Carbon* **2012**, *50* (7), 2396−2406.
(22) Hongo, H.; Yudasaka, M.; Ichihashi, T.; Nihey, F.; Iijima, S. Chemical vapor deposition of single-wall carbon nanotubes on iron-film-coated sapphire substrates. *Chem. Phys. Lett.* **2002**, *361* (3−4), 349−354.
(23) Ishigami, N.; Ago, H.; Imamoto, K.; Tsuji, M.; Iakoubovskii, K.; Minami, N. Crystal plane dependent growth of aligned single-walled carbon nanotubes on sapphire. *J. Am. Chem. Soc.* **2008**, *130* (30), 9918−9924.
(24) Ward, J. W.; Wei, B. Q.; Ajayan, P. M. Substrate effects on the growth of carbon nanotubes by thermal decomposition of methane. *Chem. Phys. Lett.* **2003**, *376* (5), 717−725.
(25) Zhang, C.; Yan, F.; Allen, C. S.; Bayer, B. C.; Hofmann, S.; Hickey, B. J.; Cott, D.; Zhong, G.; Robertson, J. Growth of vertically-aligned carbon nanotube forests on conductive cobalt disilicide support. *J. Appl. Phys.* **2010**, *108* (2), 024311.
(26) Nagaraju, N.; Fonseca, A.; Konya, Z.; Nagy, J. B. Alumina and silica supported metal catalysts for the production of carbon nanotubes. *J. Mol. Catal. A: Chem.* **2002**, *181* (1), 57−62.
(27) Amama, P. B.; Putnam, S. A.; Barron, A. R.; Maruyama, B. Wetting behavior and activity of catalyst supports in carbon nanotube carpet growth. *Nanoscale* **2013**, *5* (7), 2642−2646.
(28) de los Arcos, T.; Garnier, M. G.; Oelhafen, P.; Mathys, D.; Seo, J. W.; Domingo, C.; Garcıa-Ramos, J. V.; Sanchez-Cortes, S. Strong influence of buffer layer type on carbon nanotube characteristics. *Carbon* **2004**, *42* (1), 187−190.
(29) Wang, B.; Yang, Y.; Li, L.-J.; Chen, Y. Effect of different catalyst supports on the (n, m) selective growth of single-walled carbon nanotube from Co-Mo catalyst. *J. Mater. Sci.* **2009**, *44* (12), 3285−3295.
(30) Kudo, A.; Steiner, S. A., III; Bayer, B. C.; Kidambi, P. R.; Hofmann, S.; Strano, M. S.; Wardle, B. L. CVD growth of carbon nanostructures from zirconia: mechanisms and a method for enhancing yield. *J. Am. Chem. Soc.* **2014**, *136* (51), 17808−17817.
(31) Noda, S.; Hasegawa, K.; Sugime, H.; Kakehi, K.; Maruyama, S.; Yamaguchi, Y. Millimeter-Thick Single-Walled Carbon Nanotube Forests: Hidden Role of Catalyst Support. *Jpn. J. Appl. Phys.* **2007**, *46* (5L), L399.
(32) Willems, I.; Kónya, Z.; Colomer, J. F.; Van Tendeloo, G.; Nagaraju, N.; Fonseca, A.; Nagy, J. B. Control of the outer diameter of thin carbon nanotubes synthesized by catalytic decomposition of hydrocarbons. *Chem. Phys. Lett.* **2000**, *317* (1), 71−76.
(33) Masarapu, C.; Wei, B. Direct Growth of Aligned Multiwalled Carbon Nanotubes on Treated Stainless Steel Substrates. *Langmuir* **2007**, *23* (17), 9046−9049.
(34) Baddour, C. E.; Fadlallah, F.; Nasuhoglu, D.; Mitra, R.; Vandsburger, L.; Meunier, J.-L. A simple thermal CVD method for carbon nanotube synthesis on stainless steel 304 without the addition of an external catalyst. *Carbon* **2009**, *47* (1), 313−318.
(35) Yu, D.; Zhang, Q.; Dai, L. Highly Efficient Metal-Free Growth of Nitrogen-Doped Single-Walled Carbon Nanotubes on Plasma-Etched Substrates for Oxygen Reduction. *J. Am. Chem. Soc.* **2010**, *132* (43), 15127−15129.
(36) Amama, P. B.; Islam, A. E.; Saber, S. M.; Huffman, D. R.; Maruyama, B. Understanding properties of engineered catalyst supports using contact angle measurements and X-Ray reflectivity. *Nanoscale* **2016**, *8* (5), 2927−2936.
(37) Li, X.; Baker-Fales, M.; Almkhelfe, H.; Gaede, N. R.; Harris, T. S.; Amama, P. B. Rational Modification of a Metallic Substrate for CVD Growth of Carbon Nanotubes. *Sci. Rep.* **2018**, *8* (1), 4349.
(38) Islam, A. E.; Nikolaev, P.; Amama, P. B.; Saber, S.; Zakharov, D.; Huffman, D.; Erford, M.; Sargent, G.; Semiatin, S. L.; Stach, E. A.; Maruyama, B. Engineering the Activity and Lifetime of Heterogeneous Catalysts for Carbon Nanotube Growth via Substrate Ion Beam Bombardment. *Nano Lett.* **2014**, *14* (9), 4997−5003.
(39) Li, X. *Rational Catalyst Design for Carbon Nanotube Carpet Growth and Fischer−Tropsch Synthesis*. Doctoral Dissertation, Kansas State University, Manhattan, KS, 2019.
(40) Ganesh, I.; Bhattacharjee, S.; Saha, B. P.; Johnson, R.; Rajeshwari, K.; Sengupta, R.; Ramana Rao, M. V.; Mahajan, Y. R. An efficient MgAl2O4 spinel additive for improved slag erosion and penetration resistance of high-Al2O3 and MgO-C refractories. *Ceram. Int.* **2002**, *28* (3), 245−253.
(41) Bocanegra, S. A.; Ballarini, A. D.; Scelza, O. A.; de Miguel, S. R. The influence of the synthesis routes of MgAl2O4 on its properties

https://dx.doi.org/10.1021/acsanm.9b02509
ACS Appl. Nano Mater. 2020, 3, 1830−1840

and behavior as support of dehydrogenation catalysts. *Mater. Chem. Phys.* **2008**, *111* (2), 534−541.
(42) Gao, Y.; Kim, Y. J.; Thevuthasan, S.; Chambers, S. A.; Lubitz, P. Growth, structure, and magnetic properties of γ-Fe2O3 epitaxial films on MgO. *J. Appl. Phys.* **1997**, *81* (7), 3253−3256.
(43) Ago, H.; Nakamura, K.; Uehara, N.; Tsuji, M. Roles of Metal-Support Interaction in Growth of Single- and Double-Walled Carbon Nanotubes Studied with Diameter-Controlled Iron Particles Supported on MgO. *J. Phys. Chem. B* **2004**, *108* (49), 18908−18915.
(44) Wang, H. Y.; Ruckenstein, E. CO2 reforming of CH4 over Co/MgO solid solution catalysts — effect of calcination temperature and Co loading. *Appl. Catal., A* **2001**, *209* (1), 207−215.
(45) Li, J.; Li, J.; Zhu, Q. Carbon deposition and catalytic deactivation during CO2 reforming of CH4 over Co/MgO catalyst. *Chin. J. Chem. Eng.* **2018**, *26* (11), 2344−2350.
(46) Sehested, J.; Carlsson, A.; Janssens, T. V. W.; Hansen, P. L.; Datye, A. K. Sintering of Nickel Steam-Reforming Catalysts on MgAl2O4 Spinel Supports. *J. Catal.* **2001**, *197* (1), 200−209.
(47) Wang, F.; Li, W.-Z.; Lin, J.-D.; Chen, Z.-Q.; Wang, Y. Crucial support effect on the durability of Pt/MgAl2O4 for partial oxidation of methane to syngas. *Appl. Catal., B* **2018**, *231*, 292−298.
(48) Bing, W.; Wei, M. Recent advances for solid basic catalysts: Structure design and catalytic performance. *J. Solid State Chem.* **2019**, *269*, 184−194.
(49) Hasan, M. M.; Dholabhai, P. P.; Castro, R. H.; Uberuaga, B. P. Stabilization of MgAl2O4 spinel surfaces via doping. *Surf. Sci.* **2016**, *649*, 138−145.
(50) Lu, W.; Zu, M.; Byun, J.-H.; Kim, B.-S.; Chou, T.-W. State of the Art of Carbon Nanotube Fibers: Opportunities and Challenges. *Adv. Mater.* **2012**, *24* (14), 1805−1833.
(51) Jia, J.; Zhao, J.; Xu, G.; Di, J.; Yong, Z.; Tao, Y.; Fang, C.; Zhang, Z.; Zhang, X.; Zheng, L.; Li, Q. A comparison of the mechanical properties of fibers spun from different carbon nanotubes. *Carbon* **2011**, *49* (4), 1333−1339.
(52) Hall, W. K.; Kokes, R. J.; Emmett, P. H. Mechanism Studies of the Fischer−Tropsch Synthesis. The Addition of Radioactive Methanol, Carbon Dioxide and Gaseous Formaldehyde. *J. Am. Chem. Soc.* **1957**, *79* (12), 2983−2989.
(53) Kibby, C.; Jothimurugesan, K.; Das, T.; Lacheen, H. S.; Rea, T.; Saxton, R. J. Chevron's gas conversion catalysis-hybrid catalysts for wax-free Fischer−Tropsch synthesis. *Catal. Today* **2013**, *215*, 131−141.
(54) Tavasoli, A.; Sadagiani, K.; Khorashe, F.; Seifkordi, A. A.; Rohani, A. A.; Nakhaeipour, A. Cobalt supported on carbon nanotubes — A promising novel Fischer−Tropsch synthesis catalyst. *Fuel Process. Technol.* **2008**, *89* (5), 491−498.
(55) Zgolicz, P. D.; Stassi, J. P.; Yañez, M. J.; Scelza, O. A.; de Miguel, S. R. Influence of the support and the preparation methods on the performance in citral hydrogenation of Pt-based catalysts supported on carbon nanotubes. *J. Catal.* **2012**, *290*, 37−54.
(56) Almkhelfe, H.; Carpena-Nunez, J.; Back, T. C.; Amama, P. B. Gaseous product mixture from Fischer−Tropsch synthesis as an efficient carbon feedstock for low temperature CVD growth of carbon nanotube carpets. *Nanoscale* **2016**, *8* (27), 13476−13487.
(57) Almkhelfe, H.; Li, X.; Rao, R.; Amama, P. B. Catalytic CVD growth of millimeter-tall single-wall carbon nanotube carpets using industrial gaseous waste as a feedstock. *Carbon* **2017**, *116*, 181−190.
(58) Bedewy, M.; Meshot, E. R.; Reinker, M. J.; Hart, A. J. Population Growth Dynamics of Carbon Nanotubes. *ACS Nano* **2011**, *5* (11), 8974−8989.
(59) Futaba, D. N.; Hata, K.; Yamada, T.; Mizuno, K.; Yumura, M.; Iijima, S. Kinetics of Water-Assisted Single-Walled Carbon Nanotube Synthesis Revealed by a Time-Evolution Analysis. *Phys. Rev. Lett.* **2005**, *95* (5), 056104.
(60) Magrez, A.; Seo, J. W.; Smajda, R.; Mionić, M.; Forró, L. Catalytic CVD Synthesis of Carbon Nanotubes: Towards High Yield and Low Temperature Growth. *Materials* **2010**, *3* (11), 4871−4891.
(61) Xiong, G.-Y.; Wang, D.; Ren, Z. Aligned millimeter-long carbon nanotube arrays grown on single crystal magnesia. *Carbon* **2006**, *44* (5), 969−973.
(62) Maret, M.; Hostache, K.; Schouler, M.-C.; Marcus, B.; Roussel-Dherbey, F.; Albrecht, M.; Gadelle, P. Oriented growth of single-walled carbon nanotubes on a MgO (0 0 1) surface. *Carbon* **2007**, *45* (1), 180−187.
(63) Fu, Y.; Zhang, L.; Yue, B.; Chen, X.; He, H. Simultaneous Characterization of Solid Acidity and Basicity of Metal Oxide Catalysts via the Solid-State NMR Technique. *J. Phys. Chem. C* **2018**, *122* (42), 24094−24102.
(64) Rossi, P. F.; Busca, G.; Lorenzelli, V.; Waqif, M.; Saur, O.; Lavalley, J. C. Surface basicity of mixed oxides: magnesium and zinc aluminates. *Langmuir* **1991**, *7* (11), 2677−2681.
(65) Di Cosimo, J. I.; Apesteguía, C. R.; Ginés, M. J. L.; Iglesia, E. Structural Requirements and Reaction Pathways in Condensation Reactions of Alcohols on MgyAlOx Catalysts. *J. Catal.* **2000**, *190* (2), 261−275.
(66) Moisala, A.; Nasibulin, A. G; Kauppinen, E. I The role of metal nanoparticles in the catalytic production of single-walled carbon nanotubes—a review. *J. Phys.: Condens. Matter* **2003**, *15* (42), S3011.
(67) Song, Z.; Xu, H. Splitting methanol on ultra-thin MgO(100) films deposited on a Mo substrate. *Phys. Chem. Chem. Phys.* **2017**, *19* (10), 7245−7251.
(68) Fang, C. M.; Parker, S. C.; de With, G. Atomistic simulation of the surface energy of spinel MgAl2O4. *J. Am. Ceram. Soc.* **2000**, *83* (8), 2082−2084.
(69) Massaro, F. R.; Bruno, M.; Nestola, F. Configurational and energy study of the (100) and (110) surfaces of the MgAl2O4 spinel by means of quantum mechanical and empirical techniques. *CrystEngComm* **2014**, *16* (39), 9224−9235.

https://dx.doi.org/10.1021/acsanm.9b02509
ACS Appl. Nano Mater. 2020, 3, 1830−1840